ELSEVIER

Chemical Geology 210 (2004) 113–133

CHEMICAL GEOLOGY
INCLUDING
ISOTOPE GEOSCIENCE

www.elsevier.com/locate/chemgeo

Magmatic evolution of Li–F, rare-metal granites: a case study of melt inclusions in the Khangilay complex, Eastern Transbaikalia (Russia)

E.V. Badanina[a,*], I.V. Veksler[b], R. Thomas[b], L.F. Syritso[c], R.B. Trumbull[b]

[a] *Geological Department, SPbSU (St.-Petersburg State University), Universitetskaja emb. 7/9, St. Petersburg 1999034, Russia*
[b] *GeoForschungsZentrum Potsdam, Telegrafenberg, Potsdam 14473, Germany*
[c] *SRI (Scientific Research Institute) of Earth Crust, St. Petersburg 1999034, Russia*

Abstract

We report compositions of homogenized quartz-hosted melt inclusions from a layered sequence of Li-, F-rich granites in the Khangilay complex that document the range of melt evolution from barren biotite granites to Ta-rich, lepidolite–amazonite–albite granites. The melt inclusions are crystalline at room temperature and were homogenized in a rapid-quench hydrothermal apparatus at 200 MPa before analysis. Homogenization runs determined solidus temperatures near 550 °C and full homogenization between 650 and 750 °C. The compositions of inclusions, determined by electron microprobe and Raman spectroscopy (for H_2O), show regular overall trends of increasing differentiation from the least-evolved Khangilay units to apical units in the Orlovka intrusion. Total volatile contents in the most-evolved melts reach over 11 wt.% (H_2O: 8.6 wt.%, F: 1.6 wt.%, B_2O_3: 1.5 wt.%). Concentrations of Rb range from about 1000 to 3600 ppm but other trace elements could not be measured reliably by electron microprobe. The resulting trends of melt evolution are similar to those described by the whole-rock samples, despite petrographic evidence for albite- and mica-rich segregations previously taken as evidence for post-magmatic metasomatism.

Melt variation trends in most samples are consistent with fractional crystallization as the main process of magma evolution and residual melt compositions plot at the granite minimum in the normative Qz–Ab–Or system. However, melts trapped in the highly evolved pegmatitic samples from Orlovka deviate from the minimum melt composition and show compositional variations in Al, Na and K that requires a different explanation. We suggest that unmixing of the late-stage residual melt into an aluminosilicate melt and a salt-rich dense aqueous fluid (hydrosaline melt) occurred. Experimental data show the effectiveness of this process to separate K (aluminosilicate melt) from Na (hydrosaline melt) and high mobility of the latter due to its low viscosity and relatively low density may explain local zones of albitization in the upper parts of the granite.

Keywords: Melt inclusions; Ta; Li; F; Rare-metal granites; Orlovka; Hydrosaline melt; Immiscibility

1. Introduction

The origin of rare-metal albite-rich granites and the mechanisms of element enrichment and distribution within them have been the subject of many

* Corresponding author. Tel.: +7-812-394-8897; fax: +7-812-328-9776.
E-mail address: lena@lenusik.usr.pu.ru (E.V. Badanina).

0009-2541/$ - see front matter © 2004 Elsevier B.V. All rights reserved.
doi:10.1016/j.chemgeo.2004.06.006

studies, but controversy remains about the relative roles of magmatic and hydrothermal processes (e.g., Pollard, 1986; Cuney et al., 1992; Schwartz, 1992; Yin et al., 1995; Raimbault et al., 1995; Helba et al., 1997). The central problem is that late-stage mineral replacements and zones of hydrothermal alteration are commonly observed in these granites, making it difficult to separate the effects of igneous fractionation from post-magmatic processes. Early work on mineralized granites (e.g., Beus et al., 1962) emphasized such features and concluded that the rare-metal enrichment and other compositional peculiarities were due to metasomatism. These viewpoints were challenged by the discovery of volcanic equivalents of rare-metal granites, including the "ongonites" (topaz-bearing quartz keratophyre) in eastern Asia (Kovalenko et al., 1971), the topaz rhyolites of North America (Burt et al., 1982; Christiansen et al., 1986) and the Richemont rhyolite in France (Raimbault et al., 1995); and by experimental work that demonstrated high solubilities of ore metals in synthetic granitic liquids (e.g., London et al., 1988; Linnen et al., 1996; Linnen, 1998). However, there are still few hard facts about the behavior and composition of the melt phase in mineralized granite systems and its role in rare-metal enrichment. Several studies have demonstrated the potential of melt inclusions (MI) to shed light on this problem (Kovalenko et al., 1996; Webster et al., 1996, 1997; Thomas and Klemm, 1997; Haapala and Thomas, 2000; Thomas and

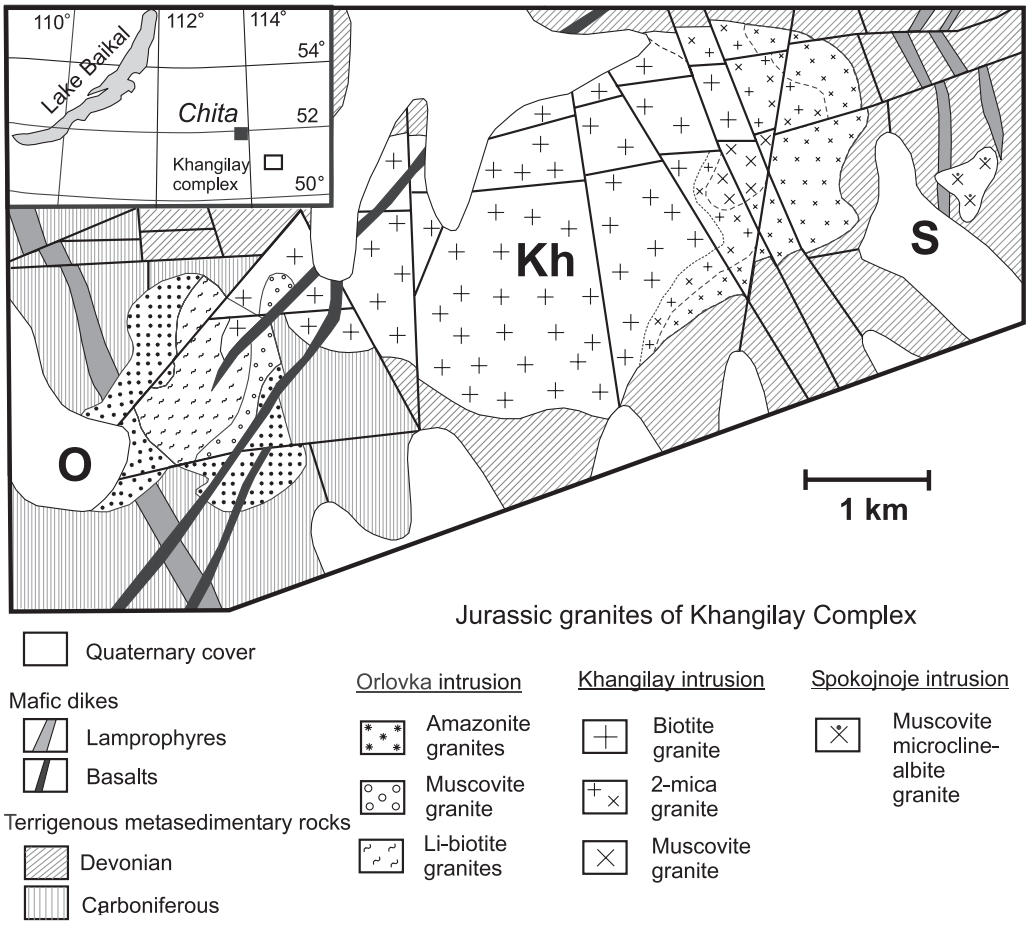

Fig. 1. Simplified geologic map of the Khangilay granite complex in eastern Transbaikalia, modified from Syritso et al., 2001.

Webster, 2000; Webster and Rebbert, 2001; Schmitt et al., 2002; Thomas et al., 2003).

This paper describes a study of melt inclusions in granites from the Late Jurassic Khangilay complex in eastern Transbaikalia, Russia (Fig. 1), which is an unusually well-developed example of a compositionally zoned, rare-metal granitic system. One of the Khangilay intrusions, Orlovka, reaches extreme levels of Li, F and Ta enrichment and is currently being mined for Ta. The granites have been thoroughly characterized in terms of rare-metal mineralization and whole-rock geochemical and petrographic composition (e.g., Zalashkova, 1969; Beskin et al., 1994; Syritso, 1993; Syritso et al., 2001). Syritso et al. (2001) suggested that the three Khangilay intrusions represent a differentiation series from a parental granite magma and supported this with the earlier finding that all three granites plot on a single Rb–Sr isochron (Kovalenko et al., 1999). However, they also pointed out textural evidence for locally intense mineral replacements and metasomatism in the Orlovka intrusion, and suggested that metasomatic processes played an important role in enriching the apical zone of the intrusion in Rb, Li and Ta. The nature of fluids involved in the proposed metasomatism and their relationship to the magma evolution are speculative, but replacement textures are indisputable and therefore, bulk-rock compositions cannot be interpreted as representing melt compositions. It is this realization that motivated the present study of melt inclusions.

Reyf et al. (2000) previously studied quartz and topaz-hosted melt inclusions from the Orlovka granite, but the small size of many inclusions prevented a detailed compositional analysis, and their study did not cover the other, less specialized units of the Khangilay complex. Our sampling of quartz-hosted melt inclusions included all major rock types in the complex, and we were able to obtain melt compositions from samples ranging from biotite granite to the highly evolved pegmatitic phases of lepidolite–albite–amazonite granite in the Orlovka intrusion. The emphasis of this paper is on the nature of the melt phase and its evolution in the system, based on major element compositions of melt inclusions determined by electron microprobe and Raman spectroscopy (for H_2O). More detailed studies are planned to determine the trace element composition of the melt inclusions, with emphasis on aspects of rare-metal enrichments, and to investigate the coexisting primary fluid inclusions in the same samples.

2. Geological setting

The Khangilay complex is located in the central part of the Aginsk Paleozoic block of Eastern Transbaikalia, one of several continental blocks that accreted to the southern margin of the Siberian craton in the middle Paleozoic. The trans-Baikal region as a whole is one of the world's most extensive areas of anorogenic granites, with plutons emplaced at various times from the Devonian to Mesozoic periods (Zanvilevich et al., 1985; Wickham et al., 1995). On the surface, granitic rocks of the Khangilay complex are exposed as three adjacent bodies (Beskin et al., 1994): the main central intrusion (Khangilay) of biotite and muscovite granites about 2.5×4 km in size, and two smaller satellites, the Orlovka to the west, composed of layered lithionite–amazonite–albite Li–F granites with associated Ta deposits, and Spokoynoye to the east, which consists of microcline–albite granites with W mineralization. Both the Khangilay intrusion and the two satellites are layered and represent strongly differentiated granitic series of rocks from parental biotite granites to pegmatite bodies and greisens (Fig. 2). Negrey et al. (1995) reported a late Jurassic Rb–Sr isochron age of 142 ± 3 Ma for the Orlovka granite and Kovalenko et al. (1999) found that samples from all three intrusions of the Khangilay complex plot on a single Rb–Sr isochron which defines an age of 142.9 ± 0.9 Ma.

The country rocks are mostly weakly metamorphosed terrigenous sediments of late Paleozoic age. There are minor differences in the country rocks surrounding the Orlovka and Spokojnoje intrusions. Orlovka is hosted by weakly metamorphosed shales and sandstones, silicic tuffs and conglomerates of upper Devonian to Carboniferous age, while the rocks around the Spokojnoje intrusion are lower Devonian metamorphosed sandstones and siltstones with minor greenstone layers. The contact zones

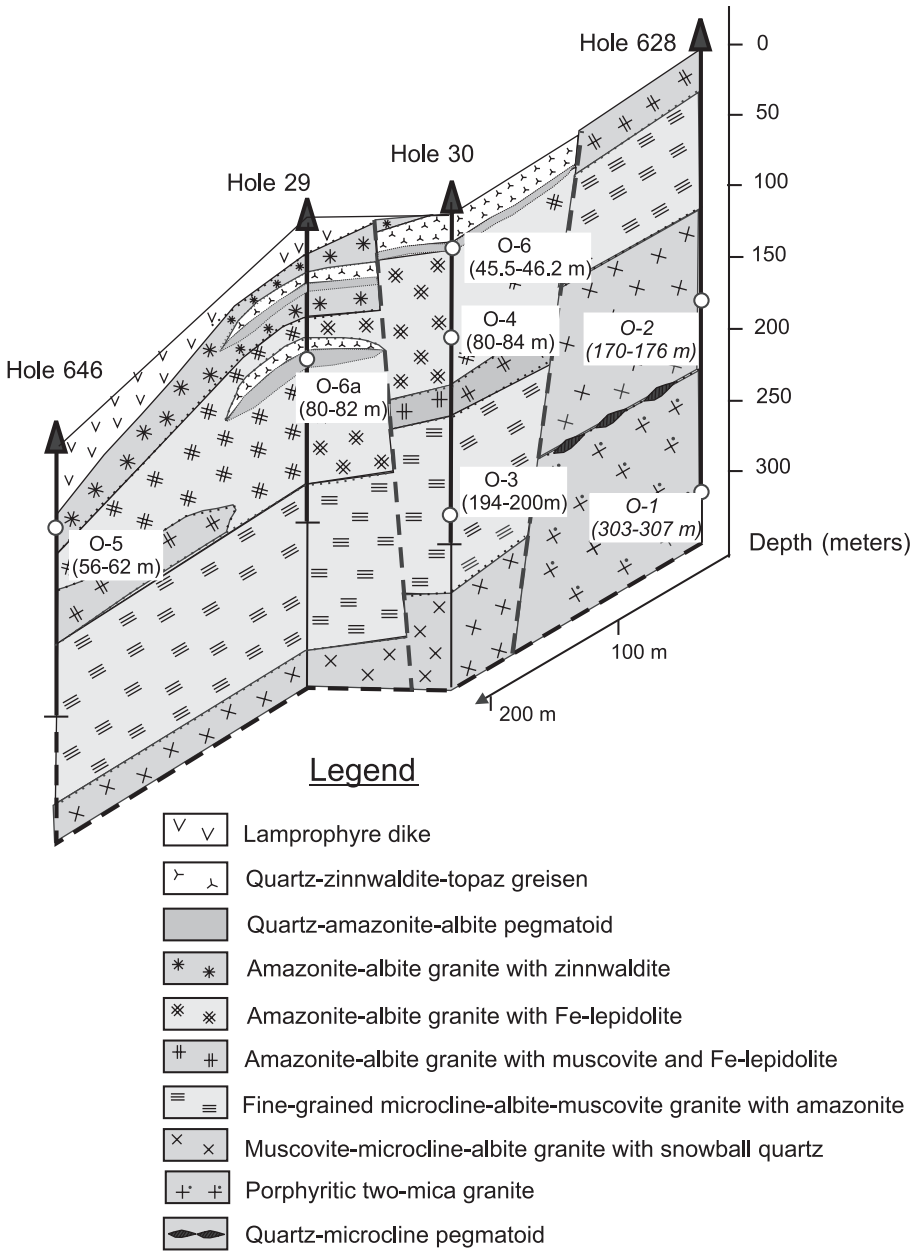

Fig. 2. Interpretative cross-section through the Orlovka intrusion showing the location of diamond drill cores and depth intervals in core where samples in this study were taken. See Appendix A for more description of lithologies in each zone.

around both intrusions are metasomatized and veined, but their mineralogic and chemical character differ. Thus, the exocontact of Spokojnoje shows development of garnet-bearing calc-silicate rocks, abundant muscovite–fluorite veins and quartz veins, which locally contain wolframite. Distinctive contact rocks around Orlovka include a zone of greisenization at the roof of the intrusion with distinctive albite–protolithionite–topaz greisen containing fluorite and beryl. External veins and

Table 1
Average whole-rock compositions of lithologic units from the Khangilay, Orlovka and Spokojnoje intrusions

Intrusion	Khangilay				Orlovka												Spokojnoje			
Unit	KH-1	S.D.	KH-2	S.D.	O-1	S.D.	O-2	S.D.	O-3	S.D.	O-4	S.D.	O-4 A	S.D.	O-5	S.D.	S-1	S.D.	S-2	S.D.
SiO_2	74.5	1.03	75.5	0.20	72.9	0.39	74.5	0.18	71.5	0.65	71.9	0.82	72.3	0.61	71.3	1.08	73.5	0.50	77.6	1.13
TiO_2	0.19	0.03	0.09	0.03	0.16	0.03	0.04	0.02	0.06	0.03	0.02	0.01	0.02	0.01	0.02	0.01	0.09	0.03	0.03	0.02
Al_2O_3	13.4	0.29	13.7	0.38	14.1	0.60	14.1	0.87	16.7	0.75	16.0	0.81	16.2	0.73	15.5	0.79	14.2	0.35	13.0	0.61
Fe_2O_3	0.86	0.12	0.35	0.10	0.65	0.25	0.55	0.11	0.38	0.12	0.49	0.30	0.52	0.33	0.46	0.12	0.68	0.10	0.54	0.12
FeO	1.09	0.22	0.90	0.39	1.07	0.43	0.39	0.03	0.43	0.44	0.59	0.37	0.56	0.29	0.38	0.22	0.62	0.22	0.37	0.06
MnO	0.03	0.01	0.03	0.01	0.04	0.01	0.07	0.03	0.09	0.07	0.26	0.09	0.46	0.10	0.22	0.10	0.06	0.02	0.17	0.06
MgO	0.41	0.17	0.44	0.06	0.36	0.11	0.32	0.10	0.15	0.10	0.16	0.05	0.15	0.04	0.24	0.17	0.22	0.12	0.22	0.10
CaO	0.64	0.17	0.16	0.03	0.75	0.24	0.33	0.23	0.26	0.15	0.22	0.11	0.32	0.18	0.38	0.23	0.74	0.07	0.15	0.02
Na_2O	3.92	0.44	4.09	0.45	4.39	0.07	4.96	0.30	6.12	0.48	5.72	0.76	5.44	0.52	5.24	0.77	3.98	0.30	3.93	0.33
K_2O	4.70	0.47	4.58	0.30	4.86	0.30	4.49	0.45	3.48	0.50	2.86	0.51	3.12	0.58	4.78	0.56	4.48	0.36	3.52	0.33
F	0.14	0.05	0.09	0.02	0.36	0.11	0.43	0.09	0.30	0.18	1.20	0.50	1.44	0.38	1.52	0.35	0.51	0.02	0.30	0.08
−O=F	0.06	0.02	0.04	0.01	0.15	0.05	0.18	0.04	0.13	0.08	0.50	0.21	0.60	0.16	0.64	0.15	0.21	0.01	0.13	0.03
L.O.I.	0.59	0.17	0.73	0.19	1.02	0.29	0.55	0.12	0.83	0.24	0.87	0.19	0.92	0.12	1.01	0.22	1.04	0.12	1.18	0.11
Total	100.3		100.5		100.1		100.1		99.8		98.6		99.4		98.9		99.4		100.6	
Sn	10	3	28	5	39	10	28	3	7	2	11	2	10	4	34	20	44	3	123	46
Ta	6	1	10	1	8	3	26	6	39	3	75	30	73	27	184	28	10	3	38	12
Sr	138	10	60	5	81	10	27	7	4	2	6	2	4	2	6	3	87	9	56	6
Li	168	12	110	15	329	77	360	102	221	156	1175	697	1526	323	2759	762	146	4	72	12
Rb	448	24	497	33	671	109	1212	223	970	329	1318	366	1232	459	2466	333	425	30	344	28
Cs	26	3	26	3	57	8	55	10	20	6	31	10	30	12	206	200	30	6	36	10

Values give averages of three samples and standard deviation (S.D.). Data from Syritso et al. (2001) and authors' unpublished analyses for Spokojnoje.
All analyses performed at the Institute for Geology and Geochronology of the Precambrian and Institute for the Earth's Crust, University of St. Petersburg.
Methods: X-ray fluorescence for major elements, Sr and Sn; FeO by titration; ion-sensitive electrode for F; flame photometry for Li, Cs, Rb; neutron activation for Ta.
Analytical uncertainty is estimated as less than 10% of the given values, or less than 15% for Ta.

dikes include fine-grained mineralized granite and quartz–amazonite lepidolite-bearing pegmatoid.

3. Compositional zoning and metasomatic features of the Khangilay complex

All three intrusions in the Khangilay complex display some vertical zoning, which increases in complexity from the Khangilay main intrusion into the more differentiated satellite intrusions. The zones have been discriminated mineralogically, with emphasis on the type(s) of mica and feldspar present. Lithologic and petrographic descriptions, mica composition and whole-rock geochemistry of the Khangilay complex have been presented by Syritso (1993) and Syritso et al. (2001). A summary description of the zones is given in Appendix A. Table 1 presents average whole-rock compositions for the different zones from Syritso et al. (2001), augmented by analyses of the Spokojnoje granite from the authors' unpublished data.

The Khangilay main intrusion consists of biotite granite in the deep exposures and two-mica granite in the upper part. The Spokojnoje intrusion is also simply zoned, with a lower unit of porphyritic muscovite granite similar to the upper Khangilay unit, an upper unit richer in albite and microcline, and a roof zone of greisen-like quartz and mica-rich granite. The Orlovka intrusion displays a highly complex zoning, which is expressed in an overall vertical layering but with important lateral variations as well (Fig. 2). The lowest part of the Orlovka sequence is composed of protolithionite 2-mica granites and above this follow a number of texturally and mineralogically distinct units dominated by amazonite, albite and Li-micas. Some transitions between the layers are gradual, but others are sharp and suggest multiple pulses of magma rather than in situ differentiation of a single magma batch. An example of such a sharp contact is that between protolithionite granite and microcline–albite granite in borehole 628 (Fig. 2) which is marked by a series of small quartz–feldspar pegmatoid lenses colored in black on the figure.

Table 2
Electron and Raman microprobe analyses of homogenized melt inclusions in quartz from the Khangilay complex

Unit	Kh-1		Kh-2		S-1		S-2		O-1		O-2		O-3	
	x (7)	S.D.	*x* (8)	S.D.	*x* (5)	S.D.	*x* (3)	S.D.	*x* (4)	S.D.	*x* (7)	S.D.	*x* (6)	S.D.
SiO_2	69.0	0.22	67.7	2.17	67.7	1.12	64.2	0.40	69.3	1.63	69.4	1.23	69.1	4.75
TiO_2	0.11	0.02	0.09	0.06	0.11	0.05	0.02	0.02	0.08	0.06	0.09	0.02	0.01	0.01
Al_2O_3	13.3	0.70	14.9	1.03	14.1	0.63	13.2	0.48	15.0	2.62	15.4	1.08	13.5	1.99
FeOt	0.56	0.08	0.75	0.50	0.64	0.11	0.27	0.21	0.29	0.20	0.73	0.11	0.32	0.15
MnO	0.06	0.03	0.12	0.10	0.05	0.03	0.12	0.07	0.06	0.03	0.25	0.07	0.13	0.09
MgO	0.08	0.03	0.08	0.07	0.08	0.05	0.04	0.03	0.10	0.06	0.03	0.02	0.02	0.01
CaO	0.70	0.18	0.16	0.12	0.99	0.87	0.17	0.05	0.48	0.16	0.53	0.05	0.10	0.08
Na_2O	3.55	0.20	3.33	0.03	2.04	0.10	3.96	0.17	3.55	0.10	3.08	0.29	4.55	0.35
K_2O	4.65	0.18	4.30	0.20	3.96	0.31	3.97	0.25	4.55	0.01	4.00	0.25	2.52	0.31
F	0.32	0.30	0.22	0.10	0.68	0.10	d.l.	–	0.42	0.07	1.33	0.04	0.23	0.10
B_2O_3	0.68	–	n.a.	–	1.14	0.05	–	–	0.56	–	0.35	0.05	0.63	–
P_2O_5	0.07	0.02	0.05	0.04	0.05	0.01	0.31	0.14	0.03	0.02	0.03	0.02	0.01	0.01
H_2O	n.a.	–	n.a.	–	n.a.	–	n.a.	–	n.a.	–	n.a.	–	n.a.	–
Total	93.13		91.70		91.57		86.33		94.39		95.27		91.19	
Rb	1220	180	997	293	869	56	1144	28	1528	37	2650	283	1272	146

H_2O by confocal Raman spectroscopy, all others by electron microprobe. x = average value, with number of inclusions in parentheses; S.D. = standard deviation; d.l. = below detection limit; n.a. = not analyzed.

Melt inclusions were homogenized before analysis in cold-seal autoclaves for 24 h at 200 MPa. Run temperatures for each sample (in °C): Kh-1: 550–650–700; Kh-2: 650–700; S-1: 550–650–700–750; S-2: 650–750; O-1: 600–650–700; O-2: 600–700; O-3: 650–750; O-4: 600–700–750; O-4a: 700; O-5: 550–650–750; O-6: 650–750; O-6a: 650–750.

*Reference materials and source: major element oxides, T1 G glass (Jochum et al., 2000); Rb, F: Macusani glass (Pichavant et al., 1987); H_2O: Westrich glass M6N (Thomas, 2000); B_2O_3: dravite (Dyar et al., 2001).

For details of the Orlovka internal units the reader is referred to Syritso (1993) and Syritso et al. (2001). In this section, we call attention to key features of the rocks that are relevant for interpretation of the melt inclusion results. The most important part of the intrusion in terms of mineralogic and geochemical specialization is the apical section. This makes up no more than 3–5% of the total intrusion but it constitutes the richest ore horizon. Typical for the apical section are subhorizontal lenses of banded aplite and pegmatoid, with thicknesses of 5–20 cm (maximum 1.5 m) and a lateral extent of several meters (maximum more than 100 m). The aplites consist of subhorizontal bands with varying modal composition; some are granitic whereas others are dominated by either albite, K-feldspar, or by a quartz–topaz–zinnwaldite assemblage. The latter is referred as greisen in previous work and in Fig. 2 although it is not certain that its origin is hydrothermal and the term may be inappropriate. The pegmatoid lenses are dominantly quartz–amazonite rocks, typically showing a comb structure with amazonite crystals up to 40 cm long growing perpendicular to the contacts. Examples of apical units sampled for this study are O-6 and O-6a from internal pegmatoid lenses and sample O-4a, which comes from a dome-like body of amazonite–granite at the southwestern flank of the intrusion. The latter contains the only known occurrence of tourmaline (indicolite–elbaite) in the complex (Badanina et al., 2003). Evidence for a magmatic origin of the apical aplite–pegmatoid lenses is the presence of steeply dipping dikes of similar pegmatoid and aplite that cut into the country rocks.

An important characteristic of the upper units from the Khangilay complex, and particularly the Orlovka intrusion, is the presence of mineral replacements. At Orlovka, replacements can be noted in most zones but they increase in intensity upwards in the intrusion. The deepest example of mineral replacements involves albitization in the zone of O-3 (Fig. 2), where fine-grained albite replaces quartz and, to a lesser extent, microcline and plagioclase of An_{5-9}. Locally, albitization leads to nearly monomineralic vuggy albitite. Farther up in the intrusion, replacements of muscovite by Fe–

O-4		O-4 A		O-5		O-6		O-6a		Reference materials*		
x (4)	S.D.	*x* (10)	S.D.	*x* (6)	S.D.	*x* (26)	S.D.	*x* (5)	S.D.	Given	Measured	S.D. (n)
66.2	2.97	61.4	1.10	67.0	0.78	65.1	2.18	69.4	1.20	58.5	59.3	0.25 (50)
0.01	0.00	0.03	0.03	0.03	0.01	0.01	0.01	0.01	0.01	0.73	0.77	0.03 (50)
12.6	0.57	16.2	2.21	12.2	0.73	13.0	1.30	12.7	0.91	17.0	17.2	0.07 (50)
0.73	0.17	0.34	0.17	0.67	0.15	0.68	0.30	0.04	0.01	6.42	6.40	0.11 (50)
0.15	0.05	0.92	0.33	0.54	0.18	0.52	0.24	0.03	0.01	0.13	0.14	0.02 (50)
0.01	0.00	0.01	0.01	0.05	0.05	0.01	0.01	0.01	0.01	3.74	3.78	0.04 (50)
0.02	0.02	0.08	0.05	0.42	0.46	0.11	0.06	0.04	0.03	7.08	7.18	0.06 (50)
3.63	0.36	4.27	0.71	3.70	0.17	1.16	0.23	3.99	0.20	3.14	2.84	0.04 (50)
3.90	0.12	3.45	0.32	2.02	0.34	5.58	0.41	3.97	0.10	1.94	1.97	0.03 (50)
0.36	0.12	1.10	0.72	1.65	0.07	1.58	0.26	d.l.	–	1.3	1.29	0.18 (22)
0.72	–	–	–	0.89	0.11	1.53	0.43	n.a.	–	10.1	10.9	0.50 (30)
0.01	0.00	0.03	0.02	0.01	0.01	0.02	0.02	0.03	0.01	0.18	0.19	0.03 (50)
7.9	0.06	n.a.	–	8.4	0.50	8.6	0.30	n.a.	–	5.11	5.03	0.57 (27)
96.28		87.90		97.62		97.86		90.17				
2169	174	2663	567	2013	211	3614	174	2288	278	1167	1184	115 (15)

lepidolite are noted, which locally produce a characteristic ocellar structure of mica intergrowths, and tartan-twinned amazonite occurs replacing albite. Topaz and ore minerals accompany the mineral replacements in places. Finally, the exocontact of Orlovka contains important metasomatic zones of greisenization and albitization of the country rocks. These greisen bodies reach up to 10 m in thickness and include distinctive zinnwaldite–topaz–albite assemblages, locally rich in honey-colored beryl. These replacement features are well known and figure prominently in existing genetic models for the Orlovka granite and its mineralization. In their interpretive model of the Khangilay complex, Syritso et al. (2001) stressed the role of igneous differentiation in producing the geochemical specialization of the Orlovka granite, but they also attributed considerable importance to post-magmatic metasomatism. They proposed that an alkalic "metasomatic front" of albitization in the mid-section of the intrusion (unit O-3) transported F, Li, Rb, Ta and Nb upwards in the granite, where they were concentrated by acidic metasomatism of the upper zone and in the exocontact. Our inclusion data show that at least some of the geochemical features attributed to metasomatism are present in the residual melts themselves.

4. Methods

4.1. Sample preparation and homogenization procedure

Selection of suitable samples for analyses was made on quartz separated from bulk rock and examined under a petrographic microscope in immersion oil or glycerine. The melt inclusions are crystalline at room temperature and had to be reheated before analysis. To avoid loss of volatiles by decrepitation and to overcome the problem of slow melting rates of daughter crystals, homogenization runs took place in rapid-quench cold-seal pressure vessels (described by Thomas et al., 2000). Quartz grains with inclusions were sealed in Au capsules of 5 mm diameter and 20 mm length and then heated for 24 h at 200 MPa and at various temperatures between 550 and 750 °C. After each run, the inclusions were again inspected optically and, if daughter crystals remained, a second aliquot of unheated quartz grains from the same sample was heated to a higher temperature. Generally, from two to four heating runs were performed and it was found necessary to heat most samples to 700 or 750 °C to achieve complete homogenization (run temperatures for each sample are listed in Table 2). This procedure produced a maximum number of homogeneous, non-decrepitated inclusions for study, but it precluded visual observation of phase changes and an accurate assessment of solidus temperatures. After successful homogenization runs, the quartz grains with inclusions were ground and polished on both sides and the doubly-polished wafers, 0.5-mm thick, were mounted in epoxy for analysis by electron microprobe.

4.2. Electron microprobe analysis

All elements except B were analysed using a Cameca SX-100 electron microprobe at the GeoForschungsZentrum Potsdam (GFZ). Analyses were performed in four-spectrometer WDS mode with 20 nA beam current and an accelerating voltage of 15 kV. The beam size was 10 μm or, where allowed by the size of inclusions, glasses were analysed with a beam size of 20–40 μm. Calibration for major elements employed synthetic oxides and natural mineral standards (wollastonite for Si, Ca; orthoclase for K, Al; albite for Na; rutile for Ti; rhodonite for Mn; hematite for Fe; apatite for P; synthetic MgO for Mg) and data reduction used the PAP scheme. A description of analytical conditions, calibration standards and estimates of analytical errors for the GFZ SX-100 facility, based on the study of MPI-DING reference glasses, is given in Jochum et al. (2000). Typical precision and accuracy values are given in Table 2. Rubidium was calibrated with synthetic Rb–feldspar crystals prepared by S. Melzer, GFZ Potsdam. Analytical accuracy was better than 10% relative, verified by analyzing chips of Macusani glass (Table 2).

Boron analysis of glass and minerals were performed using a Cameca SX-50 microprobe equipped with the PC2 pseudo-crystal and using a liquid nitrogen cold trap to minimize contamination (see Dyar et al., 2001; Thomas et al., 2003 for descrip-

tions of the SX-50 procedures and error estimates). Analytical conditions were 10 kV and 40 nA, with counting times of 60 s on peak. LaB_6 was taken as an internal standard and synthetic glasses with B_2O_3 contents up to 20 wt.% were used as external standard. The glasses (Breitländer BR F2, BR 2/L, BR 4/l, CRM glass CZ 4001, granitic glass from Thomas, 2002a; Veksler and Thomas, 2002) were cross-checked with Raman spectroscopy (see Thomas, 2002a,b). For mineral analyses, natural boromuscovite and natural reedmergerite were used as external standards. Electron microprobe and SIMS values for B_2O_3 are in excellent agreement (Thomas et al., 2003).

4.3. Raman spectroscopy

Water concentrations in homogenized melt inclusions from three samples were determined by confocal Raman spectroscopy at the GeoForschungsZentrum Potsdam using the Dilor XY Laser Raman Triple 800 mm spectrometer equipped with an Olympus optical microscope and a long-distance 80× objective. The 488 nm line of a Coherent Ar+ Laser Model Innova 70-3 and a power of 500 mW of the argon laser were used for sample excitation and spectra were collected with a Peltier-cooled CCD detector. Counting time was 50 s and 10 accumulations were used for each determination. Water contents were determined using method II of Thomas (2000) which measures the ratio of the 3550:490 cm^{-1} band intensities. Calibration employed synthetic granite, haplogranite and albite glasses whose water contents were determined by Karl–Fischer titration (see Thomas, 2000, 2002b). The relative precision and accuracy of this technique was shown to be better than 10% in the concentration range of 0.5–16 wt.% (Thomas, 2000).

5. Results

5.1. Petrography of inclusions and homogenization temperatures

Most of the quartz phenocrysts selected for the melt inclusion study were 3–5 mm in size and contained three main types of inclusions: (1) solid mineral inclusions; (2) devitrified melt inclusions; and (3) fluid inclusions. Our study concentrated solely on melt inclusions that appear to be primary from their occurrence in the core of quartz phenocrysts, their random distribution and large size. Primary-looking fluid inclusions (L + V, and, in some samples, containing birefringent daughter crystals) were noted but not investigated in any detail for this study (see also Reyf et al., 2000). Secondary melt and fluid inclusions are common along healed cracks and we made no effort to analyze them. Some of the larger primary melt inclusions are associated with tiny, single-phase fluid inclusions (L or V), which may represent trapped fluid that was lost from the melt inclusion during by partial decrepitation in nature. In several cases, a crack intersects the melt inclusion and we speculate that fracturing may have happened on cooling through the quartz alpha-beta transition temperature (the potential effect of this on inclusion composition is discussed later).

The size of melt inclusions varies from 20 to about 150 μm, with most between 50 and 100 μm. About 90 vol.% of the inclusions at room temperature are aggregates of daughter mineral phases and the rest is occupied by liquid and vapor phases (Fig. 3). In general, melt inclusions from more evolved rocks are bigger and have larger proportions of fluid phases. Melt inclusions are especially abundant in quartz from the most evolved Orlovka rock types (samples O-5 and O-6). Considerable effort was taken to identify the mineral phases in crystalline inclusions based on their optical properties, morphology and electron microprobe data. The following mineral phases were identified: albite, K-feldspar, different varieties of mica (see below), zircon, columbite, monazite and fluorite. Many of the minerals are also observed as solid inclusions in the same quartz grains as the melt inclusions. However, solid phases in the melt inclusion population of a given sample could all be completely remelted by homogenization and quenching runs at 700–750 °C, suggesting that they were not accidentally trapped, but are true daughter phases.

Syritso et al. (2001) emphasized the wide variations in mica compositions in the Khangilay complex and demonstrated that different mica types

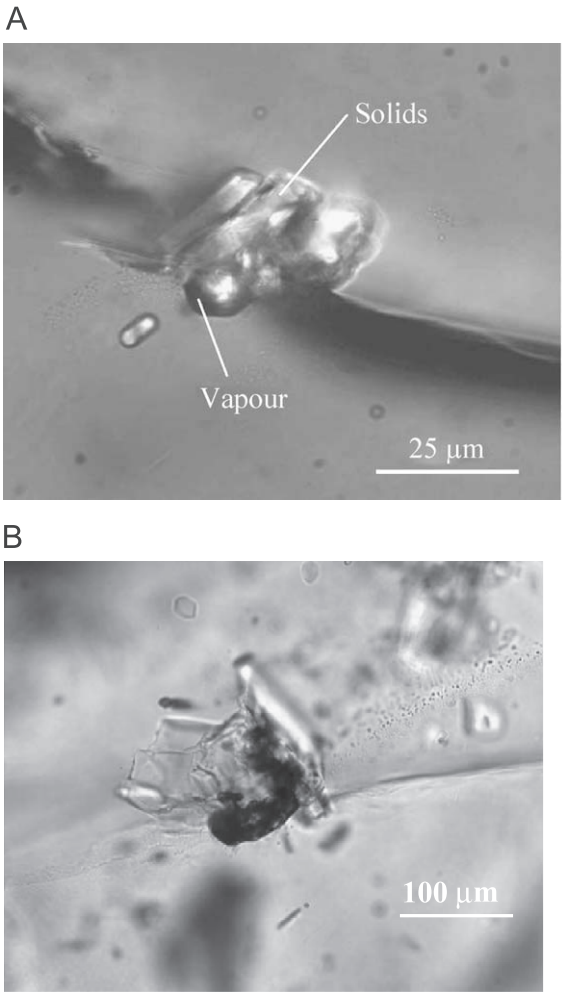

Fig. 3. Photomicrographs of quartz-hosted crystallized melt inclusions at room temperature. A. melt inclusion from Orlovka sample O-2 showing clear vapor bubble, B. melt inclusion from Spokojnoje sample S-1 where only daughter minerals are visible. Typically, over 90% of inclusion volumes consist of daughter minerals, thus the irregular angular shapes.

are a characteristic feature of granite evolution in the layered sequence, particularly at Orlovka (see Appendix A). They also pointed out that the sequence of mica compositions with differentiation in the Orlovka granite is unusual compared with several other examples of Li–F granites. The sequence begins with Li–biotite to protolithionite in the lower units (O-1), followed by Li–muscovite farther up in the sequence (O-2). Noteworthy is the strong increase in iron concentration in the micas, especially those in the upper units O3 to O6, with formation of Fe–lepidolite and zinnwaldite. The reason for this late iron enrichment is not yet understood and the interpretation of mica compositions in the bulk rocks is complicated by the replacement textures and metasomatic features mentioned above, many of which involve micas as a main component. Although our study did not focus on micas, many of the mica daughter crystals in melt inclusions and quartz hosts are large enough for microprobe analysis and this allows us to demonstrate the range of compositions in mica that was isolated from potential overprinting by metasomatism. Selected microprobe analyses of micas and K-feldspar from unheated melt inclusions from Orlovka, Khangilay and Spokojnoje are presented in Tables 3 and 4. In detail, the mica compositions are complex and there are variations between mica daughter crystals and free micas trapped during growth of the quartz host. A discussion of these features is beyond the present scope and a full treatment of magmatic and metasomatic stages of mica evolution will be the subject of a separate publication. For the present purposes, it is important only to point out that the magmatic range of mica compositions is similar to those of bulk mica from Orlovka described by Syritso et al. (2001) and in particular, the increase in Fe along with extreme values of F in the later units is not a metasomatic feature. The F concentration in some micas reaches as high as 8 wt.%, which is near the theoretical limit for complete F occupancy of the interlayer sites. Such F-rich examples appear to be characteristic for Li-, Fe-rich granites and several examples were reported by Tischendorf et al. (1997 and references therein).

5.2. Homogenization behavior and chemical composition of melt inclusions

The homogenization experiments were designed to produce homogeneous glass suitable for microprobe analyses, so we have no detailed information about the mode of homogenization and the sequence of phase changes on heating. The solidus temperature can only be roughly constrained. Several heating steps were applied for some samples

Table 3
Selected microprobe analyses of micas in crystallized melt inclusions and solid inclusions in host quartz

Unit	S-1		Kh-1			O-1				O-2					O-3		O-4a		O-4		O-5		O-6		O-6a	
Mica type[a]	mu	mu	mu	mu	bt	bt	pt	mu	mu	mu	mu	mu	mu	pt	pt	mu	lp	zw	mu	mu	mu	lp	pt	pt	zw	mu
Occurrence[b]	mi	cr	mi	cr	cr	mi	mi	mi	mi	mi	mi	cr	cr	cr	mi	cr	mi	mi	mi	cr	cr	cr	mi	mi	mi	cr
SiO_2	46.6	46.6	45.5	48.9	50.4	38.4	38.9	46.2	46.4	46.6	46.0	46.3	44.4	39.2	47.9	46.3	49.7	40.5	45.5	45.8	47.3	51.5	37.4	39.5	41.7	45.4
TiO_2	0.26	0.14	0.39	0.45	3.26	1.58	0.06	0.76	0.05	0.05	0.52	0.33	0.46	1.97	0.05	0.04	0.00	0.06	<0.01	<0.01	<0.01	0.03	0.05	0.07	0.04	0.01
Al_2O_3	31.0	33.7	32.8	29.2	11.2	21.0	22.3	27.8	26.7	34.8	29.8	28.3	28.4	16.7	36.6	37.4	19.0	14.7	35.6	34.6	37.2	19.6	22.9	24.7	24.3	35.5
FeO	4.09	2.60	1.65	4.86	19.5	20.20	17.8	7.85	6.69	1.12	5.30	4.74	6.47	21.6	2.47	0.17	5.36	20.2	0.78	1.61	0.02	5.77	23.7	19.0	12.6	0.31
MnO	0.33	0.11	0.03	0.14	0.39	0.41	1.66	0.32	0.48	0.37	0.57	1.63	1.64	0.28	0.96	0.00	2.43	5.23	0.32	0.34	0.02	1.55	2.08	1.50	1.38	1.00
MgO	0.44	0.24	0.04	1.88	4.59	4.55	0.05	1.48	0.60	0.02	0.34	0.09	0.37	4.60	0.03	0.07	0.02	0.16	0.01	0.02	0.04	0.01	0.09	0.06	0.02	<0.01
CaO	<0.01	0.02	<0.01	0.58	0.01	0.04	0.01	<0.01	<0.01	<0.01	0.02	<0.01	<0.01	<0.01	<0.01	<0.01	<0.01	<0.01	<0.01	<0.01	0.01	<0.01	0.01	0.02	<0.01	<0.01
Li_2O[c]	0.27	0.06	0.08	0.14	0.42	0.32	0.79	1.12	0.99	0.32	0.70	1.66	2.26	2.43	0.59	0.23	6.31	3.47	0.37	0.44	2.16	5.84	1.63	1.31	2.91	0.37
Rb_2O	0.14	0.08	0.13	0.15	0.21	0.21	0.91	0.56	0.42	0.39	0.67	1.24	0.70	0.05	0.47	0.26	1.17	0.90	0.42	0.49	0.23	0.72	0.64	0.66	0.65	0.66
Na_2O	0.16	0.21	0.28	1.17	0.25	0.74	0.11	0.15	0.12	0.37	0.15	0.15	0.18	0.04	0.48	0.22	0.11	0.62	0.24	0.19	0.15	0.10	0.17	0.24	0.16	0.25
K_2O	10.5	10.2	10.5	8.08	7.41	8.33	9.30	8.85	10.2	10.6	10.3	9.83	10.2	9.73	10.2	10.0	10.2	8.29	10.8	10.7	10.1	10.7	9.14	9.01	9.86	10.0
B_2O_3	1.04	n.a.	1.05	n.a.	n.a.	n.a.	n.a.	n.a.	n.a.	0.56	n.a.	n.a.	n.a.	n.a.	0.69	0.44	n.a.	n.a.	n.a.	n.a.	n.a.	n.a.	0.94	n.a.	0.81	n.a.
F	0.76	0.24	<0.1	0.45	1.19	1.43	2.48	2.19	2.01	0.86	1.54	2.96	3.74	4.92	1.35	<0.1	8.81	6.13	0.96	1.08	2.20	8.41	3.87	3.39	5.50	0.96
-O for F	0.32	0.10	0.00	0.19	0.50	0.60	1.04	0.92	0.85	0.36	0.65	1.24	1.57	2.07	0.57	0.00	3.70	2.57	0.40	0.46	0.92	3.53	1.62	1.42	2.31	0.40
Total	95.4	94.1	92.6	95.9	98.4	96.5	93.5	96.4	93.9	95.8	95.3	96.2	97.3	99.4	101.2	95.2	99.5	97.8	94.6	94.8	98.5	100.7	100.9	98.1	97.7	94.1
Structural formula based on 11 O equivalents																										
Si	3.14	3.15	3.11	3.28	3.59	2.87	3.02	3.18	3.28	3.10	3.18	3.21	3.08	2.92	3.03	3.04	3.41	3.13	3.07	3.10	3.07	3.46	2.75	2.91	2.99	3.08
Al^{IV}	0.80	0.85	0.83	0.72	0.41	1.13	0.98	0.82	0.72	0.87	0.82	0.79	0.92	1.08	0.93	0.94	0.59	0.87	0.93	0.90	0.93	0.54	1.19	1.09	0.96	0.92
B	0.06		0.06							0.03					0.04	0.02							0.06		0.05	
Z-site sum	4.00	4.00	4.00	4.00	4.00	4.00	4.00	4.00	4.00	4.00	4.00	4.00	4.00	4.00	4.00	4.00	4.00	4.00	4.00	4.00	4.00	4.00	4.00	4.00	4.00	4.00
Ti	0.01	0.01	0.02	0.02	0.17	0.09	<0.01	0.04	<0.01	<0.01	0.03	0.02	0.02	0.11	<0.01	<0.01	<0.01	<0.01	<0.01	<0.01	<0.01	<0.01	<0.01	<0.01	<0.01	<0.01
Al^{VI}	1.67	1.84	1.81	1.58	0.52	0.72	1.06	1.43	1.50	1.86	1.60	1.52	1.41	0.38	1.81	1.97	0.95	0.47	1.90	1.86	1.92	1.01	0.80	1.06	1.09	1.91
Fe	0.23	0.15	0.09	0.27	1.16	1.26	1.15	0.45	0.40	0.06	0.31	0.27	0.38	1.34	0.13	0.01	0.31	1.30	0.03	0.09	<0.01	0.32	1.46	1.17	0.75	0.02
Mn	0.02	0.01	0.00	0.01	0.02	0.02	0.10	0.02	0.03	0.02	0.03	0.09	0.09	0.02	0.05	0.00	0.13	0.32	0.02	0.02	<0.01	0.08	0.12	0.09	0.08	0.06
Mg	0.04	0.02	0.00	0.19	0.49	0.51	0.01	0.15	0.06	<0.01	0.04	0.01	0.04	0.51	<0.01	0.01	<0.01	0.02	<0.01	<0.01	<0.01	<0.01	0.01	0.01	<0.01	<0.01
Li[c]	0.07	0.02	0.02	0.04	0.09	0.12	0.30	0.31	0.28	0.09	0.19	0.46	0.63	0.83	0.15	0.06	1.88	1.21	0.10	0.12	0.29	1.72	0.57	0.46	0.95	0.10
Y-site sum	2.04	2.05	1.94	2.11	2.45	2.72	2.62	2.40	2.27	2.03	2.20	2.37	2.57	3.19	2.14	2.05	3.27	3.32	2.05	2.09	2.21	3.13	2.96	2.79	2.87	2.09
K	0.91	0.88	0.92	0.69	0.67	0.79	0.92	0.78	0.92	0.90	0.91	0.87	0.91	0.92	0.82	0.84	0.90	0.82	0.93	0.93	0.84	0.92	0.86	0.85	0.90	0.87
Na	0.02	0.03	0.04	0.15	0.03	0.11	0.02	0.02	0.02	0.05	0.02	0.02	0.02	0.01	0.06	0.03	0.02	0.09	0.03	0.03	0.02	0.01	0.02	0.03	0.02	0.03
Ca	<0.01	<0.01	<0.01	0.04	<0.01	<0.01	<0.01	<0.01	<0.01	<0.01	<0.01	<0.01	<0.01	<0.01	<0.01	<0.01	<0.01	<0.01	<0.01	<0.01	<0.01	<0.01	<0.01	<0.01	<0.01	<0.01
Rb	0.01	<0.01	0.01	0.01	0.01	0.01	0.05	0.02	0.02	0.02	0.03	0.06	0.03	<0.01	0.02	0.01	0.05	0.04	0.02	0.02	0.01	0.03	0.03	0.03	0.03	0.03
Cs	<0.01	<0.01	0.01	<0.01	<0.01	<0.01	<0.01	<0.01	<0.01	<0.01	<0.01	0.01	<0.01	<0.01	<0.01	<0.01	<0.01	<0.01	<0.01	<0.01	<0.01	<0.01	<0.01	<0.01	<0.01	<0.01
X-site sum	0.94	0.91	0.98	0.89	0.71	0.91	0.99	0.82	0.96	0.97	0.96	0.96	0.96	0.93	0.90	0.88	0.97	0.95	0.98	0.98	0.87	0.96	0.91	0.91	0.95	0.93
F	0.16	0.05	0.00	0.10	0.27	0.34	0.61	0.48	0.45	0.18	0.34	0.65	0.82	1.16	0.27	0.00	1.91	1.50	0.20	0.23	0.45	1.79	0.90	0.79	1.25	0.21

Analyses by electron microprobe with Fe reported as FeO, n.a. = not analyzed.

[a] Mica types: mu—muscovite, bt—biotite, pt—protolithionite, lp—lepidolite, zw—zinnwaldite.

[b] Occurrences: mi—within melt inclusion, cr—solid inclusion in quartz.

[c] Li values were approximated by the method of Tischendorf et al. (1997) using equations for Li–F correlation (Li–Rb for F-free micas). Y-site sums over 3.0 may be due to overestimation of Li.

Table 4
Selected microprobe analyses of potassium feldspar daughter crystals in melt inclusions

Unit	S-1	S-1	Kh-1	Kh-2	O-1	O-1	O-2	O-2	O-3	O-3	O-4	O-4	O-5	O-5	O-6	O-6
SiO_2	65.1	64.7	64.3	64.3	65.4	64.8	66.3	67.0	64.4	65.0	65.3	65.3	65.0	65.2	65.9	62.1
Al_2O_3	17.9	17.7	18.2	17.7	18.4	17.9	17.9	18.2	18.3	18.1	18.4	18.4	18.3	18.2	18.9	18.3
B_2O_3	1.08	0.47	n.a.	n.a.	0.19	n.a.	0.30	0.35	0.46	n.a.	0.26	0.25	n.a.	n.a.	0.43	0.33
FeO	<0.01	<0.01	0.02	<0.01	0.01	0.05	<0.01	0.06	<0.01	<0.01	0.03	<0.01	<0.01	0.01	0.07	1.87
CaO	<0.01	<0.01	<0.01	<0.01	<0.01	<0.01	<0.01	0.26	<0.01	<0.01	<0.01	<0.01	<0.01	<0.01	<0.01	<0.01
Na_2O	0.68	0.71	0.65	0.50	0.59	0.48	0.28	1.90	0.47	0.40	1.90	0.45	0.44	0.37	0.43	0.62
K_2O	15.5	15.7	15.2	15.4	14.9	15.5	15.2	12.5	15.6	15.7	13.9	15.9	15.6	15.5	15.5	15.3
Rb_2O	0.05	0.04	0.03	0.16	0.21	0.28	0.36	0.36	0.43	0.35	0.35	0.43	0.92	0.90	0.40	0.50
P_2O_5	0.04	0.03	<0.01	0.01	0.02	<0.01	0.02	<0.01	<0.01	0.03	<0.01	<0.01	0.02	0.03	0.03	<0.01
Sum	100.3	99.4	98.4	98.0	99.7	99.0	100.3	100.6	99.8	99.6	100.2	100.7	100.2	100.3	101.6	99.1
Cations based on 8 oxygens																
Si	2.97	3.00	3.01	3.02	3.01	3.02	3.03	3.02	2.98	3.01	2.99	2.99	3.01	3.01	2.98	2.93
Al	0.96	0.96	1.00	0.98	1.00	0.98	0.96	0.97	1.00	0.99	0.99	1.00	1.00	0.99	1.01	1.02
B	0.09	0.04	0.00	0.00	0.02	0.00	0.02	0.03	0.04	0.00	0.02	0.02	0.00	0.00	0.03	0.03
Fe	<0.01	<0.01	<0.01	<0.01	<0.01	<0.01	<0.01	<0.01	<0.01	<0.01	<0.01	<0.01	<0.01	<0.01	<0.01	0.07
Ca	<0.01	<0.01	<0.01	<0.01	<0.01	<0.01	<0.01	0.01	<0.01	<0.01	<0.01	<0.01	<0.01	<0.01	<0.01	<0.01
Na	0.06	0.06	0.06	0.05	0.05	0.04	0.02	0.17	0.04	0.04	0.17	0.04	0.04	0.03	0.04	0.06
K	0.90	0.93	0.90	0.92	0.87	0.92	0.89	0.72	0.92	0.93	0.81	0.93	0.92	0.91	0.90	0.92
Rb	<0.01	<0.01	<0.01	<0.01	0.01	0.01	0.01	0.01	0.01	0.01	0.01	0.01	0.03	0.03	0.01	0.02
P	<0.01	<0.01	<0.01	<0.01	<0.01	<0.01	<0.01	<0.01	<0.01	<0.01	<0.01	<0.01	<0.01	<0.01	<0.01	<0.01
Sum	4.98	4.99	4.97	4.97	4.95	4.97	4.94	4.93	4.99	4.98	5.00	4.99	4.99	4.98	4.97	5.04

Analyses by electron microprobe with total Fe reported as FeO.
n.a. = not analyzed.

(see Table 2) and the quenched runs indicated partial melting of inclusion contents at 550 and 600 °C (there were no runs at lower temperature). Complete homogenization occurred by 700 or 750 °C, which gives an upper estimate for the liquidus temperature at 200 Mpa.

Homogenized melt inclusions large enough for reliable microprobe analysis (diameter >20 μm) were found and studied in two samples from the Khangilay intrusion, two samples from Spokojnoje and eight samples from the Orolovka granite. Between 3 and 26 individual inclusions were measured in each sample and the average compositions with standard deviations are given in Table 2. The standard deviations for the abundant major element constituents SiO_2, Al_2O_3, Na_2O and K_2O are 10% of the mean or less and the variations of others are typically at or below 30% relative to the mean value. Thus, the inclusions in any given sample have quite uniform composition. This gives us confidence that the average compositions are good estimates of the melt composition present during quartz crystallization in the different zones of the intrusion, and that any fluid loss by partial decrepitation on cooling did not effect the major element composition significantly.

A feature of all inclusions is their low analytical totals, which is attributed to components including, mainly, H_2O (Raman analyses of selected samples show up to 8.5 wt.%, H_2O, see below) and also Li_2O (not analyzed) and perhaps also CO_2 in some cases (fluid inclusions are CO_2-bearing, see below). For comparisons of melt compositions and whole-rock, therefore, it is useful to recalculate all analyses to a volatile-free sum of 100 wt.%, and when this is done the SiO_2 contents of melt inclusions (74–78 wt.% SiO_2 with one exception) and bulk rocks overlap. Melt inclusions in all three granite intrusions are peraluminous in composition, with molar A/CNK ratios ($Al_2O_3/CaO + Na_2O + K_2O$) between 1.1 and 1.6. The sum of CaO, TiO_2, FeO and MnO concentrations is below 2 wt.% (Table 3). Melt compositions calculated in terms of normative quartz–albite–orthoclase (Fig. 4) correspond

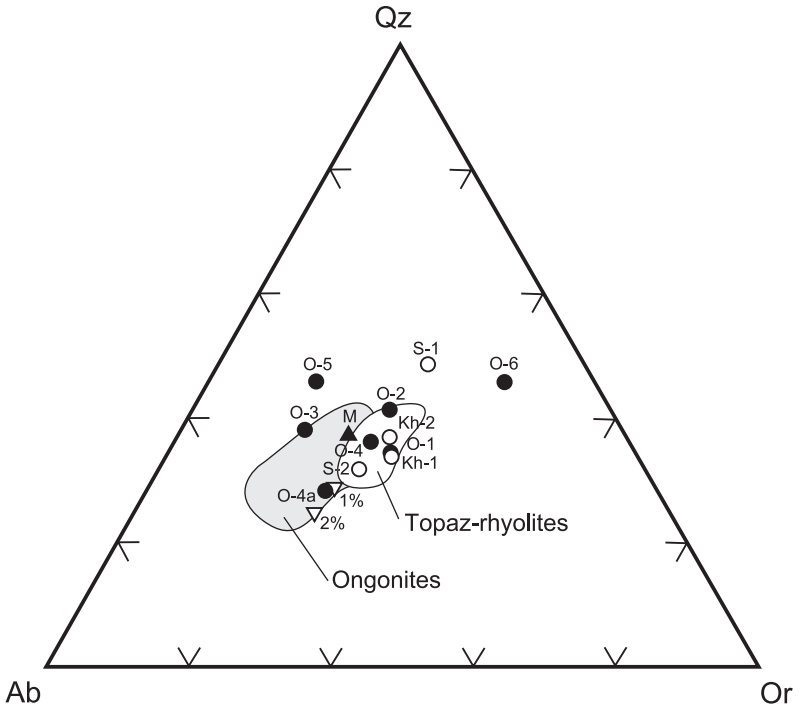

Fig. 4. CIPW normative compositions of homogenized melt inclusions in the Ab–Qz–Or projection along with compositional fields of ongonites (Kovalenko and Kovalenko, 1976), topaz rhyolites (Christiansen et al., 1986). Filled triangle marked "M" shows composition of Macusani glass from London et al. (1988) and open triangles mark the 100 Mpa minimum melt compositions in water-saturated haplogranite with 1 and 2 wt.% F added, from Manning (1981).

closely with the field for natural ongonites (Kovalenko and Kovalenko, 1976), and topaz rhyolites (Christiansen et al., 1986) and the Peruvian macusanite (London et al., 1988), as well as with experimentally determined compositions of low-pressure minimum melts in water-saturated haplogranite (Manning, 1981). Three samples (O-5, O-6 and S-1) plot outside the field of ongonite, topaz rhyolite and haplogranite. The samples have higher normative Qz and quite wide variations in the Ab/Or ratios. The deviation from minimum melt composition is not thought to be an analytical problem since, particularly for sample O-6, a large number of inclusions were measured and all show similar compositions. A possible interpretation of these anomalous melt compositions is explored in the discussion section.

The concentration of volatile components B_2O_3 and F show a 3-fold increase in the melts from the Khangilay granite to the upper Orlovka granite, with a total range for each component of about 0.5 to 1.5 wt.%. These are average values for inclusions in each sample (Table 2), whereas the extreme values from single inclusions are 2.8 wt.% F and 2.1 wt.% B_2O_3. Fluorine and B concentrations correlate poorly in the samples, and one reason for their different behavior is likely to be that F is a major or essential constituent in the crystallizing assemblage whereas B is not. Fluorine minerals include topaz and fluorite, and F is also extremely abundant in some micas (Table 3), so its concentration in the residual melt will depend on the local crystallizing assemblage. By contrast, no minerals are present with B as an essential component (very scarce tourmaline was found in only one sample, O-4A), and B remains incompatible in the melt with differentiation. In fact, because of the lack of B-minerals in the Orlovka granite or exocontact greisens, the high B values in the melt inclusions were unexpected. The mineral hosts for

B in the bulk rocks are not presently known, but the micas and feldspar are likely to be important judging from the fact that inclusion daughter minerals contain up to 1 wt.% B_2O_3 (Tables 3 and 4). High F values for the Orlovka granite had been reported by Reyf et al. (2000), but their results suggested 2 to 6 wt.% F. The discrepancy could reflect the fact that Reyf et al. (2000) analyzed small melt inclusions hosted in topaz and the high F contents may not be representative of the melt because of either overheating during homogenization runs or excitation of the host mineral during microprobe analysis. The concentration of H_2O in the homogenized melt inclusions was determined in samples O-4, O-5 and O-6, which represent the most highly evolved units of the Orlovka granite so the values obtained may be considered as maxima for the complex. Analyses were made by confocal Raman spectroscopy and yielded 7.9 to 8.6 wt.% H_2O (Table 2). Added together, the volatile components B, F and H_2O in the most differentiated melts at Orlovka, therefore, make up over 11 wt.%. Chlorine contents in most inclusions are below detection limit. We did not analyze for CO_2 in this study but the presence of primary CO_2–H_2O fluid inclusions in some samples suggests that it is a significant component in the melt. Reyf et al. (2000) reported a molar proportion of H_2O to CO_2 of about 92% to 8% in fluid inclusions which they interpreted as being magmatic.

The concentrations of Rb in the melt inclusions range from about 1000 to 3600 ppm and show a fairly regular increase from the Khangilay to Spokojnoje granites and upwards in the Orlovka-layered sequence. Unfortunately, most other trace elements are below detection limit of the electron microprobe. One aspect of particular interest are the Ta concentrations in the melt since tantalite occurs in several of the Orlovka units and the granite is mined for Ta. Experimental studies of manganotantalite solubility in granitic melts by Linnen and Keppler (1997) and Linnen (1998) suggest saturation levels of 500–1400 ppm Ta in water-saturated haplogranite melt at 600 °C, or as high as 2000–4000 ppm in melts containing 1 wt.% each of Li_2O and F. Whole-rock Ta values from Orlovka (Table 1) reach 184 ppm, similar to the levels in other mineralized Ta granites (e.g., Beauvoir with 300 ppm: Raimbault et al., 1995, Yichun with 195 ppm: Yin et al., 1995; Nuweibi with 155 ppm: Helba et al., 1997). We routinely analyzed melt inclusions for Ta, but the highest value obtained (800 ppm) is below detection limit for our procedure (2300 ppm Ta at the 3σ level). Thus, we cannot report the Ta concentrations in the residual melts using this method, but the results do rule out Ta values in the 2000–4000 ppm range suggested for saturation in F- and Li-rich granites by Linnen (1998). More work is clearly needed, and a focus for further study will be on the trace element concentrations in the melt inclusions.

6. Discussion

6.1. Are inclusions representative of the melt?

Before discussing the implications of the inclusion data for evolution of the Khangilay complex, it is necessary to justify the assumption that inclusion compositions are representative of the melt phase and were not changed after trapping. We believe this is the case because of the following arguments. First, many inclusions are large enough (>50 μm) to avoid the problem of chemical gradients in the melt around growing phenocrysts (Lu et al., 1995). Second, the composition of individual inclusions from a given sample are quite uniform (Table 3). Third, melt inclusion compositions plotted in the Q–Ab–Or projection fall in the field of natural quenched melts (ongonites) and the minimum granite. Finally, the variation in melt inclusion composition with position in the layered granites is systematic and regular, and fits the expected trends for residual melts during granitic differentiation (Fig. 5 and following discussion). There may be a problem with SiO_2 values caused by overheating and dissolution of host quartz during homogenization runs. All homogenization runs had temperatures of 700 or 750 °C and the same duration of 24 h, but the melt compositions differ greatly between the Khangilay biotite granites and Orlovka F-, Li-rich amazonite granite, so it is likely that the more evolved melt inclusions have been overheated. High SiO_2 caused by overheating is suggested by the Qz–Ab–Or projection (Fig. 4) where samples S-1,

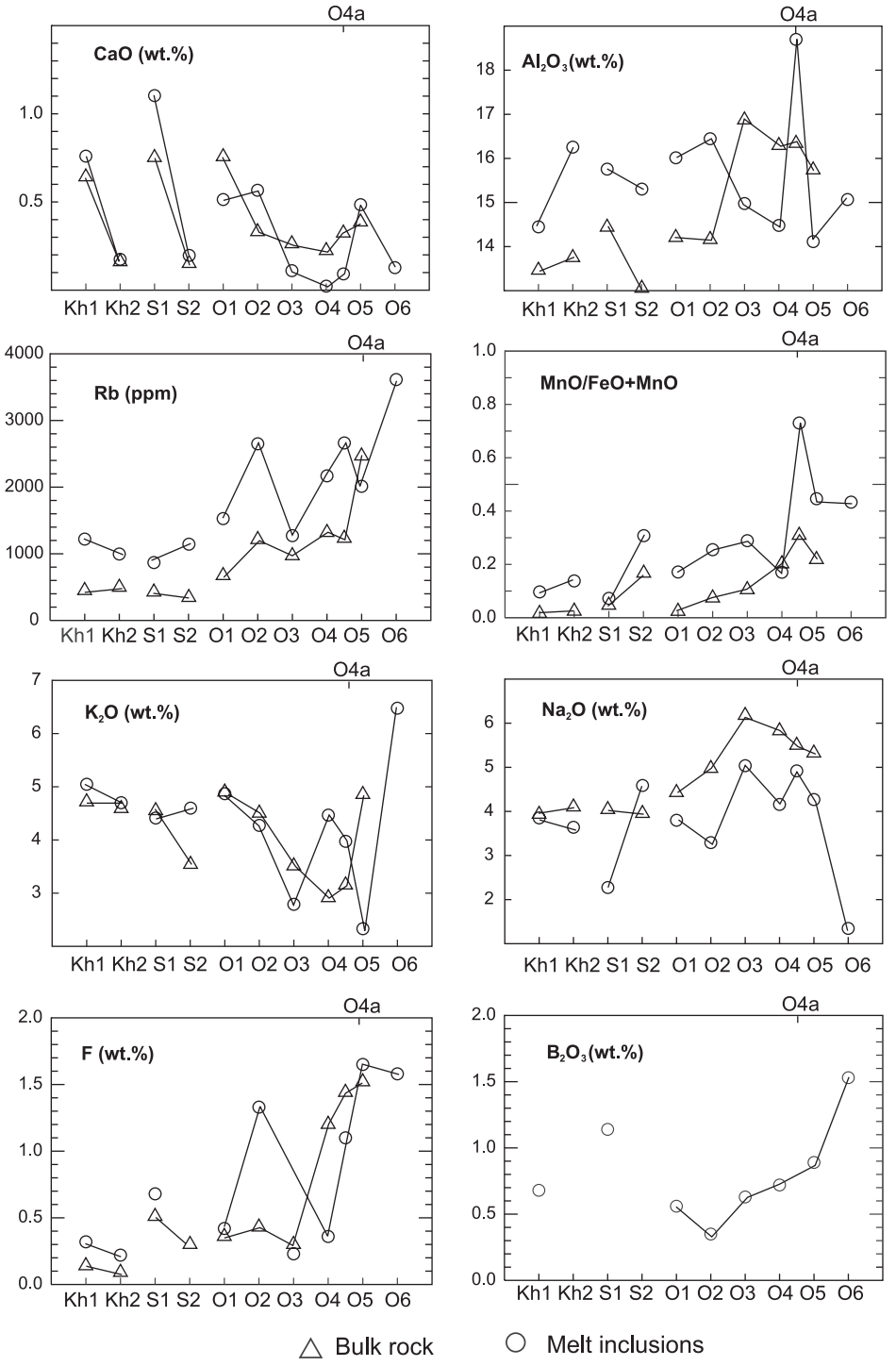

Fig. 5. Compositions of homogenized melt inclusions and corresponding bulk rocks (all data normalized to 100% analytical sum) from different petrographic units of the Khangilay, Spokojnoje and Orlovka granites. The sequence of units from left to right corresponds to their relative order of emplacement or vertical succession in the intrusions (see Figs. 1 and 2).

O-5 and O-6 have excess Qz compared with the other samples and the reference ongonites and topaz rhyolites. Note that samples O-5 and O-6 are the most evolved melts in the Orlovka system, with 11 wt.% combined F, B_2O_3 and H_2O.

6.2. Melt evolution

The main result of this work is the documentation of melt evolution throughout the sequence of units in the Khangilay complex, from the Khangilay to the Spokojnoje granites and through the layered Orlovka sequence O-1 to O-6. This evolution is illustrated in Fig. 5 on plots of composition against the position of samples in the complex, along with the corresponding whole-rock compositions (Table 1). The melt inclusion data show overall trends of increasing F, Rb, B_2O_3 and MnO/MnO + FeO with decreasing CaO from early to late units in the complex (toward the right in Fig. 5) and this is consistent with the established sequence of differentiation suggested by earlier studies of bulk-rock samples. Both sets of data show a good correspondence and in most samples the melt composition is more differentiated than the respective rock, which is reasonable considering that melt compositions are residual with respect to the solid assemblage at the time of trapping. There are also several differences in the variation trends between bulk-rock and melt inclusions apparent in Fig. 5. These are neither surprising nor easy to interpret when considering that the bulk-rock compositions average several meters of drillcore and will reflect any lithologic factors like mineral accumulations and replacements, whereas the inclusions represent a kind of "snapshot" of melt present at the particular location and time where the host quartz crystallized. A complicating factor is that quartz growth in the granites likely occurs over a considerable range of crystallization, so different increments of residual melt could be trapped in one or more grains from a given sample. This may explain some of the variation in inclusion compositions from single samples (compare standard deviation values in Table 2). There is also the possibility that partial decrepitation occurred above the solidus in some samples, leading to a loss of volatiles as suggested by clusters of fluid inclusions around large melt inclusions. This process could lead to reduced B and F in the inclusions and contribute to heterogeneity in those components. In all, however, the magnitude of internal variations is not large enough to put doubt on the average values on which this discussion is based. However complex, the inclusion compositions represent residual melts that were present when quartz in the respective units was crystallizing, so the variations shown in Fig. 5 are features of the magma.

We consider now the compositional data from the Orlovka intrusion in terms of the layered sequence shown in Fig. 2 and with reference to the Khangilay and Spokojnoje samples. The geologic observations within the Orlovka intrusion suggest an important difference in the nature of units represented by O-1 and O-2 compared with those that follow upward in the sequence (O-3 to O-6). The lower units are fairly homogeneous protolithionite and muscovite granites, whereas the units represented by samples O-3 to O-5 show replacement features involving amazonite, albite and micas, as described above. Sample O-6 is from an amazonite–quartz pegmatite lens in unit O-5. The geochemical data show significant breaks between samples O-2 and O-3 in terms of several components and one can divide the samples on this basis into two groups. The melt inclusions in Orlovka O-1 and O-2 samples, and in samples from Khangilay and Spokojnoje display compositional variations close to those of bulk rock samples and they are consistent with trends expected for conventional fractionation of a granitic magma. From O-2 to O-3, there is a sharp drop in Rb and F contents, as well as in Al_2O_3, and an increase in Na_2O which accords with the albite enrichments in the later units. As a group, samples O-3 to O-6 show far less regular trends in composition than the first group in terms of the alkali elements, Al, F and Rb, and the two groups also contrast in terms of the relationships between bulk-rock and melt inclusion compositions. Whereas in the Kh-1 to O-2 samples the melt has consistently higher F and Al_2O_3 than bulk rock and nearly identical K_2O contents, the relationships are the opposite or variable for samples O-3 to O-5. A poorer correspondence between bulk rock and melt inclusions in the more evolved units is not unexpected considering the common mineral replacement textures in these rocks, and it was this evidence

which led to suggestions that these units were strongly affected by metasomatism. However, we find that the melt inclusions from these units also show strong variations in many of the major components, particularly K_2O and Na_2O, and therefore the cause of metasomatism (fluid or melt) needs to be considered critically.

The compositional trends represented by melt inclusions for many of the components and samples examined are consistent with a fractional crystallization control for much of the granite sequence of the Khangilay complex, as concluded by Syritso et al. (2001). Fractionation should produce residual melts near the water-saturated minimum in a Qz–Ab–Or projection (Fig. 4) and this criterion is fulfilled for melt inclusion compositions from most samples. The exceptions are S-1, O-3, O-5 and O-6, which have high normative Qz and variable Ab/Or ratios. The problem of overheating during homogenization of the melt inclusions could cause a shift to higher normative Qz, and there is a chance that inclusions of the most-evolved melts were heated above their liquidus temperature as described above. However, this would not affect the Ab/Or ratios. It is also difficult to envisage any crystallization scenario in a granite system that could explain the variations in Al_2O_3, K_2O and Na_2O in the later Orlovka units or the sharp changes in F and Rb concentration. The greatest deviation from an expected residual melt composition is in pegmatite sample O-6. This sample is the most highly fractionated in the sequence in terms of F (matched by O-5), Rb, B_2O_3 and H_2O, and it has the lowest Na_2O and highest K_2O contents of all samples studied. We are confident that the average composition for O-6 is representative of a residual melt because inclusions are abundant in the sample and 26 individual inclusions showed the same compositional features (Table 2). Therefore, sample O-6 and to a lesser extent O-3 to O-5 as well, present melt compositions that defy explanation by any reasonable crystal-melt fractionation model. Other possibilities, like post-trapping interaction with the quartz host, incomplete daughter mineral homogenization, partial decrepitation or heterogeneous trapping of melt and a solid phase offer no satisfactory solution because it is unreasonable that these factors could operate in the same way for all the several inclusions measured in each sample.

We believe the explanation for the unusual features of melt evolution late in the Orlovka system lies in unmixing of the residual melt into two liquid phases that have strongly different affinities for K and Na. Liquid immiscibility in volatile-rich evolved granites is not a currently favored process for melt evolution, but there is good evidence for it from recent experiments on synthetic B-, F- and P-rich granite (Veksler and Thomas, 2002; Veksler et al., 2002; Veksler, 2004, this volume). These studies were stimulated by melt inclusion evidence for liquid immiscibility in F-, P-rich pegmatites (e.g. Thomas et al., 2000), in a system which is not strictly analogous to the low-P Orlovka composition. The experiments demonstrated stable coexistence of three fluid phases at geologically realistic conditions of 700 °C and 50–100 MPa: aluminosilicate melt, dilute, low-density aqueous fluid and a salt-rich dense fluid (hydrosaline melt), which may be dominated by alkali chlorides, fluorides, hydrated silicates, borates, phosphates or carbonates depending on the bulk composition of the system. The experiments also demonstrated that Na partitions strongly into hydrosaline melts and K favors the aluminosilicate melt. The chemical effect of immiscibility is likely to go together with a mechanical segregation because of large differences in viscosity and density between the conjugate melts. This coupled mechanism offers a simple and attractive explanation for the unusual chemical compositions of highly evolved residual melts (e.g., sample O-6 and O-5) and for the K-rich and Na-rich mineral segregations observed in apical zones of the massif. Furthermore, the coexistence of a hydrosaline melt with an aqueous fluid will favor high-temperature hydrolysis reactions (see Veksler, 2004, this volume), which can explain the common association of greisenization (H-metasomatism) with albitization in mineralized granites. It is tempting to speculate that melt separation and hydrolysis are the reason for the association of lens-like bodies of banded aplite with pegmatoid in the Orlovka roof zone, where albite-rich and K-feldspar-rich compositions coexist with greisen-like quartz–topaz–mica rocks (Fig. 2). Kortemeier and Burt (1988) postulated a similar scenario, with late-stage separation of a hypersaline B–Na-

rich melt, to explain the association of quartz–topaz dikes and ongonite dikes in the Flying Ranch locality, Arizona.

The immiscibility hypothesis is unconfirmed for Orlovka at present because the coexisting fluid inclusions in Orlovka samples have not yet been studied in detail. However, a first indication for carbonate-rich and borate-rich magmatic fluids was found in primary fluid inclusions from a quartz–topaz-rich segregation in amazonite granite from the endocontact zone, eastern flank. Unpublished Raman analyses of two inclusion types from this sample revealed up to 35 wt.% of $NaHCO_3$ and up to 15 wt.% H_3BO_3, respectively.

7. Conclusions

This study of melt inclusions from the layered granites of the Khangilay complex document the composition of residual melt evolution in a classic example of F–Li- and rare-metal rich granite systems. The most characteristic features of the homogenized melt inclusions are their high volatile contents, which in the most-evolved melts reach over 11 wt.% (H_2O: 8.6 wt.%, F: 1.6 wt.%, B_2O_3: 1.5 wt.%). Concentrations of Rb range to 3600 ppm but other trace elements could not be analyzed by electron microprobe and will be the focus of a separate study.

The melt inclusion compositions show regular differentiation trends for major elements and Rb similar to those described for the corresponding whole-rock compositions (Syritso et al., 2001). In general, the major-element compositions of trapped melts are consistent with experimental compositions of the granite minimum at low pressure in the normative Qz–Ab–Or system, thus supporting our interpretation that the inclusions reliably represent residual melt compositions. However, deviations from the minimum-melt compositions were found in quartz from the most-evolved pegmatitic units in the apical zone of the Orolovka intrusion. Melts trapped in sample O-6 have extremely K-rich compositions and those in O-5 are enriched in Na relative to the granite minimum. It is difficult to envision a crystal fractionation process that would produce these contrasting trends in alkali ratio at the last stages of melt evolution. Instead, we suggest that the inclusion compositions reflect a process of unmixing between a Na–F-rich hydrosaline melt and K-rich aluminosilicate melt, as has been recently demonstrated experimentally (Veksler et al., 2002) and inferred in several previous studies of high-temperature granitic ore systems and pegmatites.

Like many others of its class, the Orlovka rare-metal granite displays abundant evidence for mineral replacements involving feldspar and mica components in particular, and the conventional interpretation has been that metasomatism (albitization, greisenization) played a major role in the granite evolution and, particularly, ore formation. This study has not yet resolved the relative importance of magmatic and hydrothermal processes for albite- or mica-rich zones in Orlovka, but our inclusion data demonstrate that effective separation of Na and K did occur in the residual melts. Based on these results and recent experimental studies in compositionally similar systems, we believe that aluminosilicate–hydrosaline melt immiscibility is a geologically relevant process in evolved granites, and we predict that further inclusion studies at Orlovka and similar occurrences elsewhere will uncover more evidence of its petrologic and metallogenetic significance.

Acknowledgements

Thanks to Dieter Rhede and Oona Appelt (GFZ Potsdam) for help with microprobe analyses and Gerhard Berger (GFZ Potsdam) for polished sections. Wilhelm Heinrich (GFZ Potsdam) gave access to the hydrothermal lab and has steadily encouraged our melt inclusion work. E.V.B. acknowledges E.V. Volkova (SRI Earth Crust, St. Petersburg) for geologic information and V.I. Kovalenko (IGEM Moscow) for stimulating discussions. The research was supported by the Russian Foundation for Basic Research (01-05-64985), the Russian Ministry of Higher Education (PD02-1.5-289), the Deutsche Forschungsgemeinschaft (Th 489/2–3 and 436 RUS 17/83/01) and the Deutsche Akademische Austauschdienst. Reviews by Donald Burt, Daniel Kontak and Robert Linnen were very helpful. **[SG]**

Appendix A. Lithologic description and modal composition of granite units in the Khangilay complex

Sample/ unit[a]	Unit thickness in drill-core	Main lithology	Modal composition (vol.%)[b]	Mica type	Accessories
Kh-1	unknown	porphyritic biotite granite (Kspar to 3 cm with smoky quartz)	Qz: 29, Ksp: 46, Pl: 16 (An_{24-10}), Bt: 8, Mu: 2	biotite, rare secondary muscovite	ilmenite, apatite, zircon, monazite, ± euxenite
Kh-2	unknown	weakly porphyritic medium-grained muscovite leucogranite	Qz: 36, Ksp: 40, Pl: 18 (An_{10-12}), Mu: 6	Li-phengite, muscovite	apatite, zircon, fluorite, euxenite, cassiterite, wolframite
O-1	Ca. 30 m	weakly porphyritic m.g. two-mica granite	Qz: 26–38, Ksp: 24–32, Pl: 22–29 (albite and An_{15-17}), Bt: 2–5, Mu: 8–15	Li-biotite (protolithionite), Li–Fe– muscovite	zircon, apatite, monazite, Ta–Nb– rich rutile
O-2	20 to 150 m mean: 85 m	porphyroblastic m.g. muscovite–microcline–albite granite with snowball quartz	Qz: 28–35, Ksp: 21–28, Pl: 31–36 (albite and An_{5-9}), Mu: 6–12	Li–Fe– muscovite	zircon, apatite, fluorite, Ta–rutile, columbite
O-3	30 to 100 m: mean 60 m	equigranular, f.g. microcline–albite–muscovite granite with rare amazonite	No modal analysis; albitization common (Ab to 66%), local vuggy albitite	green muscovite	fluorite, monazite, cassiterite, Fe–Mn– hydroxides, ± wolframite, apatite, columbite
O-4	110 m	amazonite–albite granite with Fe–lepidolite	Qz: 12–30, Amz: 7–16, Ab: 20–60, Lep: 3–12, Topaz: 0.5–4	Fe–lepidolite (cryophyllite) after green muscovite	topaz, monazite, fluorite, tantalite, sphalerite, zircon, apatite,microlite
O-4a	unknown in core-surface sample	pegmatitic amazonite–albite granite with Fe–lepidolite, smoky snowball quartz	Qz: 12–30, Amz: 7–16, Ab: 20–60, Lep: 3–12, Tourmaline: 0.5–2, Beryl: 0.5–4	Fe–lepidolite (cryophyllite)	topaz, monazite, tantalite, Li–cryptomelane, tourmaline, beryl
O-5 west	10 m	albite–amazonite granite with snowball quartz	Qz: 10–48, Ab: 25–62, Amz: 5–36, Lep: 4–28, Topaz: 2–12	lepidolite	beryl, tourmaline, topaz, monazite, sphalerite, tantalite, cassiterite,zircon, microlite
O-5 east	5 to 30 m mean 20 m	albite–amazonite granite with zinnwaldite und fluorite	like O-5 west except for mica type	zinnwaldite	monazite, fluorite, tantalite, apatite microlite, sphalerite, zircon
O-6, O-6a	max. 7 m	Qz–Amazonite pegmatoid	no modal analysis	zinnwaldite	Like O-5
S-1	>100 m	weakly porphyritic m.g. muscovite leucogranite	Qz: 37, KFsp: 36, Pl: 20 (An_{10-12}), Mu: 6	muscovite	apatite, zircon, fluorite, garnet, wolframite
S-2	250 m	equigranular, f.g. Mu–Ab–granite	Qz: 32, Ab: 44, Kfsp: 16, Mu: 8	muscovite	fluorite, apatite, garnet, wolframite

[a] The same designation is used for sample and lithologic unit. Thicknesses give here are averages from drillcore intersections. Locations of drillholes and sampling intervals are shown in Fig. 2.

[b] Modal analysis based on point-counting thin sections stained for K-feldspar. Abbreviations: f.g.—fine-grained, m.g.—medium-grained, Qz—quartz, Ab—albite, Pl—plagioclase, Ksp—K-feldspar (generally microcline), Mu—muscovite, Bt—biotite, Amz—amazonite, Lep—lepidolite, Zinn—zinnwaldite.

References

Badanina, E.V., Thomas, R., Syritso, L.F., Veksler, I.V., Trumbull, R.B., 2003. High boron concentration in an Li–F granitic melt. Dokl. Earth Sci. 390, 529–532.

Beskin, S.M., Grebennikov, A.M., Matias, V.V., 1994. The Khangilay granite pluton and related Orlovka tantalum deposit, Transbaikalia. Petrologia 2, 68–87.

Beus, A.A., Severov, E.A., Sitnin, A.A., Subbotin, K.D., 1962. Albitized and Greisenized Granites (Apogranites). Akad. Nauk SSSR, Moscow. In Russian.

Burt, D.M., Sheridan, M.F., Bikun, J.V., Christiansen, E.H., 1982. Topaz rhyolites—distribution, origin and significance for exploration. Econ. Geol. 77, 1818–1836.

Christiansen, E.H., Sheridan, M.F., Burt, D.M., 1986. The geology and geochemistry of Cenozoic topaz rhyolites from the western United States. Spec. Pap. - Geol. Soc. Am. 205, 82 p.

Cuney, M., Marignac, C., Weisbrod, A., 1992. The Beauvoir topaz–lepidolite–albite grantie (Massif Central, France): the disseminated magmatic Sn–Li–Ta–Nb–Be mineralization. Econ. Geol. 87, 1766–1794.

Dyar, D., et al., 2001. Reference minerals for the microanalysis of light elements. Geostand. Newslett. 25, 441–463.

Haapala, I., Thomas, R., 2000. Melt inclusions in quartz and topaz of the topaz granite from Eurajoki, Finland. J. Czech Geol. Soc. 45, 149–154.

Helba, H., Trumbull, R.B., Morteani, G., Khalil, S.O., Arslan, A., 1997. Geochemical and petrographic studies of Ta mineralization in the Nuweibi albite granite complex, Eastern Desert, Egypt. Miner. Depos. 32, 164–179.

Jochum, K.P, Dingwell, D.B., Rocholl, A., Stoll, B., Hofmann, A.W., et al., 2000. The preparation and preliminary characterisation of eight geological MPI-DING reference glasses for in-situ microanalysis. Geostand. Newslett. 24, 87–133.

Kortemeier, W.T., Burt, D.M., 1988. Ongonite and topazite dikes in the Flying Wranch area, Tonto Basin, Arizona. Am. Mineral. 73, 507–523.

Kovalenko, V.I., Kovalenko, N.I., 1976. Ongonites. Nauka, Moscow. In Russian.

Kovalenko, V.I., Kuz'min, M.I., Antipin, V.S., Petrov, L.L., 1971. Topaz-bearing keratophyre (ongonite), a new variety of subvolcanic igneous vein rock. Dokl. Earth Sci. 199, 132–135.

Kovalenko, V.I., Tsaryeva, G.M., Naumov, V.B., Hervig, R.L., Newman, S., 1996. Magma of pegmatites from Volhynia: composition and crystallization parameters determined by magmatic inclusion studies. Petrology 4, 277–290.

Kovalenko, V.I., Kostitsyn, Yu.A., Yarmolyuk, V.V., 1999. Magma sources and isotope (Sr and Nd) evolution of rare-metal Li–F granitoids. Petrology 7, 401–429.

Linnen, R.L., 1998. The solubility of Nb–Ta–Zr–Hf–W in granitic melts with Li and Li+F: constraints for mineralization in rare metal granites and pegmatites. Econ. Geol. 93, 1013–1025.

Linnen, R.L., Keppler, H., 1997. Columbite solubility in granitic melts: consequences for the enrichment and fractionation of Nb and Ta in the earth's crust. Contrib. Mineral. Petrol. 128, 213–227.

Linnen, R.L., Pichavant, M., Holtz, F., 1996. The combined effects of fO_2 and melt composition on SnO_2 solubility and tin diffusivity in haplogranitic melts. Geochim. Cosmochim. Acta 60, 4965–4976.

London, D., Hervig, R.L., Morgan, G.B., 1988. Melt-vapor solubilities and elemental partitioning in peraluminous granite–pegmatite systems: experimental results with Macusani glass at 200 MPA. Contrib. Mineral. Petrol. 99, 360–373.

Lu, F., Anderson, A.T., Davis, A.M., 1995. Diffusional gradients at the crystal/melt interface and their effect on the composition of melt inclusions. J. Geol. 103, 591–597.

Manning, D.A.C., 1981. The effect of fluorine on liquidus phase relationships in the system Qtz–Ab–Or with excess water at 1 kbar. Contrib. Mineral. Petrol. 76, 206–215.

Negrey, E.V., Zhuravlev, A.Z., Kovalenko, V.I., Yarmoluk, V.V., Shatagin, K.N., 1995. Isotopic (Rb–Sr, ^{18}O) studies of tantalum-bearing lithium–fluorine granite. Dokl. Akad. Nauk 342, 522–525 (in Russian).

Pichavant, M., Valencia Herrera, J., Boulmier, S., Briqueu, L., Joron, J.L., Jutueau, L., Marin, L., Michard, A., Sheppard, S.M.F., Trieul, M., Vernet, M., 1987. The Macusani glasses, SE Peru: evidence of chemical fractionation in peraluminous magmas. In: Mysen, B.O. (Ed.), Magmatic Processes: Physicochemical Principles. The Geochemical Society Special Publications 1, University Park, pp. 359–373.

Pollard, P.J., 1986. Geologic characteristics and genetic problems associated with the development of granite-hosted deposits of tantalum and niobium. In: Möller, P., Cerny, P., Saupe, F. (Eds.), Lanthanides, Tantalum and Niobium. Springer, Berlin, pp. 240–256.

Raimbault, L., Cuney, M., Azencott, C., Duthou, J.L., Joron, J.L., 1995. Geochemical evidence for a multistage magmatic genesis of Ta–Sn–Li mineralization in the granite at Beauvoir, French Massif Central. Econ. Geol. 90, 548–576.

Reyf, F.G., Seltmann, R., Zaraisky, G.P., 2000. The role of magmatic processes in the formation of banded Li–F-enriched granites from the Orlovka tantalum deposit, Transbaikalia, Russia: microthermometric evidence. Can. Mineral. 38, 915–936.

Schmitt, A.K., Trumbull, R.B., Dulski, P., Emmermann, R., 2002. Zr–Nb–REE mineralization in peralkaline granites from the Amis complex, Brandberg (Namibia): evidence for magmatic pre-enrichment from melt inclusions. Econ. Geol. 97, 399–413.

Schwartz, M.O., 1992. Geochemical criteria for distinguishing magmatic and metasomatic albite-enrichment in granitoids—examples from the Ta–Li granite Yichun (China) and the Sn–W deposit Tikus (Indonesia). Miner. Depos. 27, 101–108.

Syritso, L.F., 1993. Geochemical aspects of zoning of rare-metal granite massifs. Zap. Vseross. Mineral. Obsestva 2, 35–55 (in Russian).

Syritso, L.F., Tabuns, E.V., Volkova, E.V., Badanina, E.V., Vysotskii, Yu.A., 2001. Model for the genesis of Li–F granites in the Orlovka massif, Eastern Transbaikalia. Petrology 3, 268–289.

Thomas, R., 2000. Determination of water contents of granite melt inclusions by confocal laser Raman microprobe spectroscopy. Am. Mineral. 85, 868–872.

Thomas, R., 2002a. Determination of the H_3BO_3 concentration in fluid and melt inclusions in granite pegmatites by laser Raman microprobe spectroscopy. Am. Mineral. 87, 56–68.

Thomas, R., 2002b. Determination of water contents in melt inclusions by laser Raman spectroscopy. In: De Vivo, B., Bodnar, R.J. (Eds.), Workshop-Short Course on Volcanic Systems, Geochemical and Geophysical Monitoring. Melt Inclusions: Methods, Applications and Problems. September 26–30, Napoli, Italy, Proceedings Volume, A. DeFrede, via Mezzocannone, 69, Napoli, Italy, pp. 211–216.

Thomas, R., Klemm, W., 1997. Microthermometric study of silicate melt inclusions in Variscan granites from SE Germany: volatile contents and entrapment conditions. J. Petrol. 38, 1753–1765.

Thomas, R., Webster, J.D., 2000. Strong tin enrichment in a pegmatite-forming melt. Miner. Depos. 35, 570–582.

Thomas, R., Webster, J.D., Heinrich, W., 2000. Melt inclusions in pegmatite quartz: complete miscibility between silicate melts and hydrous fluids at low pressure. Contrib. Mineral. Petrol. 139, 394–401.

Thomas, R., Förster, H.-J., Heinrich, W., 2003. The behaviour of boron in a peraluminous granite–pegmatite system and associated hydrothermal solutions: a melt and fluid inclusion study. Contrib. Mineral. Petrol. 144, 457–472.

Tischendorf, G., Gottesmann, B., Förster, H.J., Trumbull, R.B., 1997. On Li-bearing micas: estimating Li contents from microprobe analyses and an improved diagram for graphical representation. Mineral. Mag. 61, 809–834.

Veksler, I.V., 2004. Liquid immiscibility and its role at the magmatic-hydrothermal transition: a summary of experimental studies. Chem. Geol.

Veksler, I.V., Thomas, R., 2002. An experimental study of B-, P- and F-rich synthetic granite pegmatite at 0.1 and 0.2 GPa. Contrib. Mineral. Petrol. 143, 673–683.

Veksler, I.V., Thomas, R., Schmidt, C., 2002. Experimental evidence of three coexisting immiscible fluids in synthetic granite pegmatite. Am. Mineral. 87, 775–779.

Webster, J.D., Rebbert, C.R., 2001. The geochemical signature of fluid-saturated magma determined from silicate melt inclusions in Ascension Island granite xenoliths. Geochim. Cosmochim. Acta 65, 123–136.

Webster, J.D., Burt, D.M., Aguillion, R.A., 1996. Volatile and lithophile trace-element geochemistry of heterogeneous Mexican tin rhyolite magmas deduced from compositions of melt inclusions. Geochim. Cosmochim. Acta 60, 3267–3283.

Webster, J.D., Thomas, R., Rhede, D., Foerster, H.J., Seltmann, R., 1997. Melt inclusions in quartz from an evolved peraluminous pegmatite: Geochemical evidence for strong tin enrichment in fluorine- and phosphorus-rich residual liquids. Geochim. Cosmochim. Acta 61, 2589–2604.

Wickham, S.M., Litvinovsky, B.A., Zanvilevich, A.N., Bindeman, I.N., 1995. geochemical evolution of Phanerozoic magmatism in Transbaikalia, East Asia: a key constraint on the origin of K-rich silicic magmas and the process of cratonization. J. Geophys. Res. 100, 15641–15654.

Yin, L., Pollard, P.J., Hu, S., Taylor, R.G., 1995. Geologic and geochemical characteristics of the Yichun Ta–Nb–Li deposit, Jiangxi Province, China. Econ. Geol. 90, 577–585.

Zalashkova, N.E., 1969. A zoning of metasomatically altered tantalum-bearing granites (apogranites). In: Subbotin, K.D. (Ed.), Mineralogical–Geochemical and Genetic Features of Rare-Metal Apogranite. Nauka, Moscow, Russia, pp. 5–29. In Russian.

Zanvilevich, A.N., Litvinovsky, B.A., Andreev, G.V., 1985. Mongolia—Transbaikalian Alkaline Granitoid Province Nauka, Moscow. 232 pp. (In Russian).